XI International Conference on Computational Plasticity. Fundamentals and Applications
COMPLAS XI
E. Oñate, D.R.J. Owen, D. Peric and B. Suárez (Eds)

COMPARATIVE INVESTIGATION AND APPLICATION OF 3D CONSTITUTIVE MODELS FOR CONCRETE

Bernhard Valentini and Günter Hofstetter

Unit for Strength of Materials and Structural Analysis
Institute of Basic Sciences in Civil Engineering
University of Innsbruck
Technikerstraße 13, A-6020 Innsbruck, Austria
e-mail: Guenter.Hofstetter@uibk.ac.at, www.uibk.ac.at/bft/

Key words: concrete model, constitutive model, concrete structure, finite element method, numerical simulation

Abstract. This contribution deals with a comparative investigation of two 3D material models for concrete. The models under consideration are a modified version of the Extended Leon model and the damage-plasticity model proposed by Grassl and Jirásek. The results of extensive comparisons of the model response with test data motivated some modifications of both concrete models, in particular, regarding the evolution of damage.

1 INTRODUCTION

Several 3D constitutive models for concrete were proposed in the last decade. E.g., Pivonka [2] developed a modified version of the Extended Leon model [1], which is formulated within the framework of plasticity theory, and applied it to the numerical simulation of pull-out tests of anchor bolts. Schütt [3] proposed a non-smooth multi-surface damage-plasticity model and employed it for the analysis of composite structures. Huber [4] compared a 3D multi-surface plasticity model for concrete with a 3D gradient enhanced damage model. Recently, a 3D concrete model, based on a combination of plasticity theory and damage theory, was proposed by Grassl and Jirásek [5].

This contribution focuses on a comparative investigation of the modified Extended Leon model [2] and the damage-plasticity model [5]. To this end, the models are implemented into the commercial FE-analysis program system ABAQUS [6] by means of a return mapping algorithm, which is enhanced by substepping and error-control in order to improve robustness and accuracy of the stress update.

The results of extensive validation of the model response by material tests motivated some modifications of both concrete models, in particular, regarding the evolution of

damage. Furthermore, the numerical simulation of a well-known 3D benchmark test demonstrates the capabilities of an enhanced version of the damage-plasticity model for the analysis of concrete structures.

2 3D CONSTITUTIVE MODELS FOR CONCRETE

2.1 Modified Extended Leon Model

The Extended Leon model is a single-surface plasticity model with nonlinear hardening and softening. It was developed by Etse [1] and modified later by Pivonka [2]. The latter version is described and employed in this paper.

The yield function of the Extended Leon (EL) model

$$f_{EL}(\sigma^m, \rho, \theta; \alpha_h, \alpha_s) = \left[\frac{1 - q_h(\alpha_h)}{f_{cu}^2}\left(\sigma^m + \frac{\rho\, r(\theta)}{\sqrt{6}}\right)^2 + \sqrt{\frac{3}{2}}\frac{\rho\, r(\theta)}{f_{cu}}\right]^2 + \\ + \frac{q_h^2(\alpha_h)}{f_{cu}} m_s(\alpha_s)\left(\sigma^m + \frac{\rho\, r(\theta)}{\sqrt{6}}\right) - q_h^2(\alpha_h)\, q_s(\alpha_s) \tag{1}$$

is formulated in terms of the hydrostatic stress σ^m, the deviatoric radius ρ, the Lode angle θ, the strain-like internal hardening variable α_h and the strain-like internal softening variable α_s; f_{cu} denotes the uniaxial compressive strength of concrete and $r(\theta)$ a deviatoric shape function, with the limiting cases of a triangular and circular yield function in the deviatoric plane.

The plastic strain rate is described by a flow rule, which is associated in the deviatoric plane and non-associated in the meridional plane.

Hardening behavior of the Extended Leon model is described by the normalized strength parameter

$$q_h(\alpha_h) = \begin{cases} q_{h_0} + (1 - q_{h_0})\sqrt{\alpha_h\,(2 - \alpha_h)} & \text{if } \alpha_h < 1 \\ 1 & \text{if } \alpha_h \geq 1 \end{cases}, \tag{2}$$

where $q_{h_0} = f_{cy}/f_{cu}$ denotes the initial value of q_h, which represents the ratio of the elastic limit stress under compressive loading, f_{cy}, and the uniaxial compressive strength.

The evolution law of the strain-like internal hardening variable is given as

$$\dot{\alpha}_h(\sigma^m, \rho, \theta; \alpha_h, \alpha_s) = \frac{\|\dot{\boldsymbol{\varepsilon}}^p\|}{x_h(\sigma^m)} = \dot{\gamma}\, h_h(\sigma^m, \rho, \theta; \alpha_h, \alpha_s) \tag{3}$$

with $x_h(\sigma^m)$ denoting the hardening ductility parameter, which increases with increasing hydrostatic pressure. Hence, the rate of the internal hardening variable α_h is decreasing for increasing values of the confining pressure.

Softening behaviour is controlled by the decohesion parameter

$$q_s(\alpha_s) = \begin{cases} 1 & \text{if } \alpha_h < 1 \\ e^{-(\alpha_s/\alpha_u)} & \text{if } \alpha_h \geq 1 \end{cases} , \tag{4}$$

which is driven by the strain-like internal softening variable α_s; $\alpha_u = G_f^I/(l_{char}\, f_{tu})$ is employed for regularizing the softening behavior with G_f^I as the specific mode I fracture energy of concrete, l_{char} as the characteristic length of the finite element and f_{tu} as the uniaxial tensile strength.

The evolution law of the strain-like internal softening variable α_s is defined as

$$\dot{\alpha}_s(\sigma^m, \rho, \theta; \alpha_h, \alpha_s) = \frac{\| \langle \dot{\boldsymbol{\varepsilon}}^p \rangle \|}{x_s(\sigma^m)} = \dot{\gamma} h_s(\sigma^m, \rho, \theta; \alpha_h, \alpha_s) \ , \tag{5}$$

with $x_s(\sigma^m)$ denoting the softening ductility parameter depending on the maximum value of the mean stress.

The friction parameter m_s in (1) is defined as

$$m_s(\alpha_s) = \begin{cases} m_0 & \text{if } \alpha_h < 1 \ , \\ m_r - (m_r - m_0)\, q_s(\alpha_s) & \text{if } \alpha_h \geq 1 \end{cases} , \tag{6}$$

where m_0 and m_r are the initial and the residual friction parameter, respectively.

2.2 Damage-plasticity model by Grassl and Jirásek

The damage-plasticity model by Grassl and Jirásek [5] is a single-surface model with nonlinear isotropic hardening, formulated within the framework of plasticity theory, and nonlinear isotropic softening, described on the basis of damage theory. The yield function of the damage-plasticity (DP) model is given in terms of the effective mean stress $\bar{\sigma}^m$, the effective deviatoric radius $\bar{\rho}$ and the effective Lode angle $\bar{\theta}$ and the strain-like internal hardening variable α_p:

$$\begin{aligned} f_{p,DP}(\bar{\sigma}^m, \bar{\rho}, \bar{\theta}; \alpha_p) = & \left[\frac{1 - q_h(\alpha_p)}{f_{cu}^2} \left(\bar{\sigma}^m + \frac{\bar{\rho}}{\sqrt{6}} \right)^2 + \sqrt{\frac{3}{2}} \frac{\bar{\rho}}{f_{cu}} \right]^2 + \\ & + \frac{m_0\, q_h^2(\alpha_p)}{f_{cu}} \left(\bar{\sigma}^m + \frac{\bar{\rho}}{\sqrt{6}} r(\bar{\theta}) \right) - q_h^2(\alpha_p) \ . \end{aligned} \tag{7}$$

The shape of the yield function in the deviatoric plane is controlled by a deviatoric shape function $r(\bar{\theta})$; m_0 denotes a friction parameter. The plastic strain rate is described by a flow rule, which is non-associated in both the deviatoric and the meridional plane.

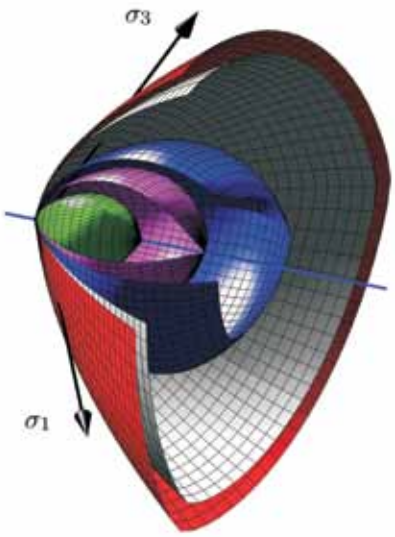

Figure 1: Yield surface of the damage-plasticity model by Grassl and Jirásek, plotted in the principal stress space for five different states during hardening

Hardening is described by the normalized strength parameter

$$q_h(\alpha_p) = \begin{cases} q_{h_0} + (1 - q_{h_0})\,\alpha_p \left(\alpha_p^2 - 3\alpha_p + 3\right) & \text{if } \alpha_p < 1 \\ 1 & \text{if } \alpha_p \geq 1 \end{cases} . \tag{8}$$

The evolution of the strain-like internal hardening variable is given as

$$\dot{\alpha}_p(\bar{\sigma}^m, \bar{\rho}, \bar{\theta}; \alpha_p) = \frac{\|\dot{\boldsymbol{\varepsilon}}^p\|}{x_h(\bar{\sigma}^m)} 4\cos^2(\bar{\theta}) = \dot{\gamma} h_p(\bar{\sigma}^m, \bar{\rho}, \bar{\theta}; \alpha_p) \tag{9}$$

with the hardening ductility parameter $x_h(\bar{\sigma}^m)$, defined in a different manner from the Extended Leon model (cf. [5]). The yield surface (7) in the principal stress space is shown for five different states during hardening in Fig. 1.

Softening material behavior of the damage-plasticity model is described by an isotropic damage law. The damage loading function is formulated in the strain-space as

$$f_{d,DP}(\boldsymbol{\varepsilon}, \boldsymbol{\varepsilon}^p; \alpha_d) = \tilde{\varepsilon}(\boldsymbol{\varepsilon}, \boldsymbol{\varepsilon}^p) - \alpha_d \ , \tag{10}$$

where $\tilde{\epsilon}$ represents the equivalent strain and α_d the strain-like internal softening variable.

Since the original version of the evolution law of the damage variable produces sharp bends of compressive stress-strain curves at the transition from hardening to softening, it is replaced in the present work by

$$\omega(\overline{\sigma}_d^m; \alpha_d) = 1 - X(\overline{\sigma}_d^m) \frac{1}{\left(1 + \dfrac{\alpha_d}{\varepsilon_{f,t}}\right)^2} - \left[1 - X(\overline{\sigma}_d^m)\right] e^{-\left(\alpha_d/\varepsilon_{f,c}\right)^2} \tag{11}$$

with $\varepsilon_{f,t}$ and $\varepsilon_{f,c}$ controlling the slope of the softening curve and

$$X(\overline{\sigma}_d^m) = \begin{cases} 0 & \text{if } \overline{\sigma}_d^m \leq -\frac{f_{cu}}{3} \\ \frac{3\overline{\sigma}_d^m}{f_{cu}} + 1 & \text{if } -\frac{f_{cu}}{3} < \overline{\sigma}_d^m < 0 \\ 1 & \text{if } \overline{\sigma}_d^m \geq 0 \end{cases} \tag{12}$$

determining the weight of the second and third term in (11) on the damage variable. Since $\overline{\sigma}_d^m$ is equal to the effective mean stress at the onset of softening, X is a constant parameter. For tensile loading with $\overline{\sigma}_d^m \geq 0$ the shape of the softening curve is controlled only by the hyperbolic function which results in a steeper initial descent of the softening envelope. In contrast, for compressive loading with $\overline{\sigma}_d^m \leq -\frac{f_{cu}}{3}$ the shape of the softening curve is controlled only by the quadratic exponential function. Thus, the sharp bend of stress-strain curves at the transition from hardening to softening, produced by the original damage law, is avoided. For $-\frac{f_{cu}}{3} < \overline{\sigma}_d^m < 0$ multi-axial combined tension-compression loading is controlled by a combination of both functions.

The rate of the strain-like internal softening variable is given as

$$\dot{\alpha}_d = \begin{cases} 0 & \text{if } \alpha_p < 1 \\ \dfrac{\dot{\varepsilon}^{p,vol}}{x_s(\dot{\varepsilon}^{p,vol})} & \text{if } \alpha_p \geq 1 \end{cases}, \tag{13}$$

where $\dot{\varepsilon}^{p,vol} = \dot{\varepsilon}_{ij}^p \, \delta_{ij}$ denotes the volumetric plastic strain rate and the softening ductility parameter $x_s(\dot{\varepsilon}^{p,vol})$ controls the evolution of the strain-like internal softening variable.

3 STRESS UPDATE ALGORITHM

For both concrete models the implicit backward Euler method is employed for integrating the constitutive rate equations. The resulting nonlinear system of equations is solved at each integration point for the stresses, the internal variables and the consistency parameters by means of Newton's method. The consistent (damage-)elasto-plastic tangent moduli are employed for achieving a quadratic rate of asymptotic convergence at the structural level.

In order to increase the robustness of the stress update for larger strain increments the return mapping algorithm is enhanced by a substepping method proposed by Pérez-Foguet et al. [7]. It is characterized by subdividing the total strain increment of the time step under consideration into m subincrements and performing the return mapping algorithm consecutively for all subincrements of the total strain increment by analogy to the well known single step method. Fig. 2 shows a comparison of the robustness of the single-step return mapping algorithm with the subincremented version of the return mapping algorithm for a set of trial stresses consisting of a grid of 51×51 equally spaced points. The grid is defined by $\sigma_m^{trial} = [-80, 20]$ N/mm^2, $\rho^{trial} = [0, 40]$ N/mm^2 and

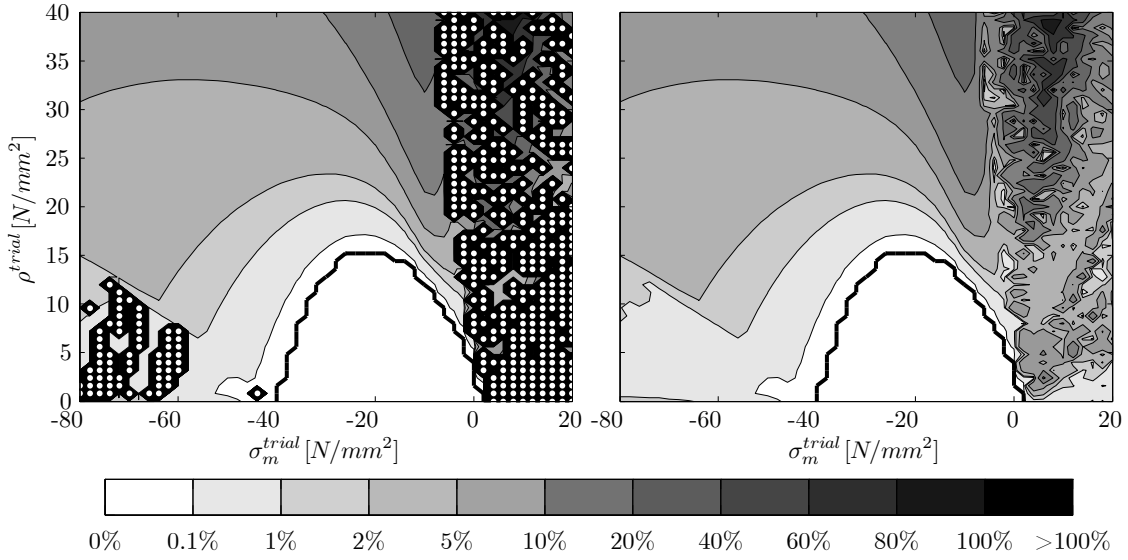

Figure 2: Iso-error maps for the stress update by the single-step Newton method (left) and the Newton method with subincrementation (right); white dots indicate points with failure of convergence

$\theta^{trial} = \pi/3$. For all stress points of this grid the initial values of the stresses, internal variables and damage variables are chosen as zero.

Fig. 2 clearly shows that in contrast to the single-step stress update, the stress update with subincrementation converges for all investigated trial stresses. In the hardening region the relative errors of the stresses are increasing with increasing distance from the boundary of the elastic domain, indicated in Fig. 2 by the black curve. In the softening domain the relative errors are larger than in the hardening domain because the nonlinearity of the underlying problem in tension is more pronounced than in compression.

In order to avoid larger integration errors as shown in Figure 2 (right), the size of the initial subincrement is determined according to a user-defined error threshold value for the stresses. To this end, for the time step under consideration two solutions for the stresses are computed based on different subincrement sizes. If the relative error of the stresses is smaller than the user-defined threshold value, then the solution is accepted, otherwise the number of subincrements is increased.

The single step integration and the subincrement integration mainly differ by the computation of the consistent tangent moduli, since the latter method requires additional terms resulting from the variation of the stresses and internal variables of the previous subincrement [7, 8] and, in addition, the consistent tangent moduli for the actual subincrement depend on those of the previous subincrement. Hence, computing the consistent elasto-plastic tangent moduli for the substepping method is more expensive than computing those for the single-step method.

4 VALIDATION AND APPLICATION

The modified Extended Leon model by Pivonka and the damage-plasticity model by Grassl and Jirásek were validated by experimental data of several test series on concrete specimens subjected to different stress paths, which are available in the literature. The investigation is documented in [8]. This validation confirmed the superiority of the damage-plasticity model. In the following, exemplarily, only a comparison of the results of triaxial compression tests with different levels of confinement, described in [9], with the respective model response is presented.

In a further validation step the modified damage-plasticity concrete model is applied to the numerical simulation of well-known 3D benchmark tests, including cylindrical concrete specimens subjected to torsional loading, cyclic loading tests of RC squat bridge columns and tests on beam-shaped concrete specimens, subjected to combined bending and torsional loading. In the following, only the latter benchmark test is addressed briefly. The analysis of all benchmark tests is documented in [8].

4.1 Validation by material tests

The material parameters of the concrete specimens, tested by Imran and Pantazopoulou [9], are given in Table 1. In this table G_f^I is estimated according to [10] from the maximum aggregate size of $d_{max} = 10$ mm.

Table 1: Material parameters for the triaxial compression tests according to [9]

parameter	(mean) value	
E_c	30000.00	N/mm^2
ν_c	0.15	
f_{cu}	47.40	N/mm^2
f_{tu}	4.74	N/mm^2
G_f^I	0.0780	Nmm/mm^2

Fig. 3 shows a comparison of experimental data and the computed response for triaxial compression tests with different levels of confinement. The peak stresses at different levels of confinement are predicted well by both models. However, the modified Extended Leon model (ELM) underestimates both, the axial and lateral strain, in particular, for higher levels of confinement.

In contrast to the modified Extended Leon model, the damage-plasticity model (DPM) by Grassl and Jirásek yields good agreement of measured and predicted axial and lateral strains for different levels of confinement. A further slight improvement is achieved by the enhanced softening law (11), as the artificial sharp bends are eliminated (DPM-enh.).

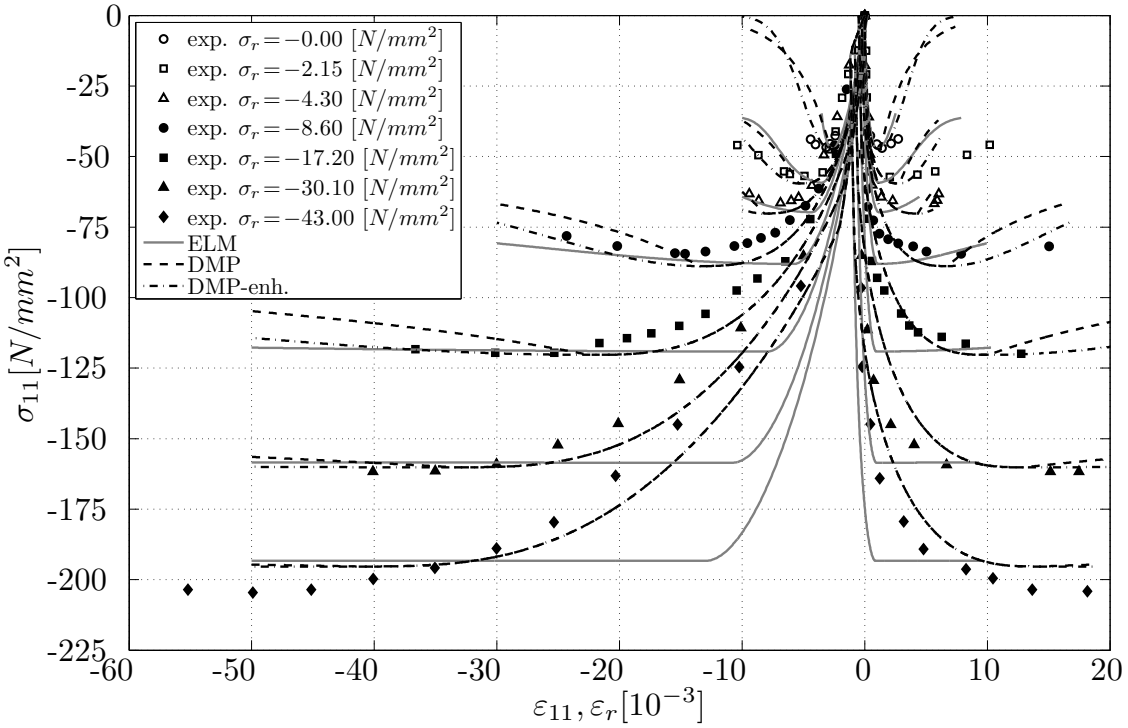

Figure 3: Experimental and numerical results of triaxial compression tests according to [9]

4.2 Benchmark test: the PCT-3D test

In the PCT-3D tests, conducted at the University of Innsbruck, prismatic concrete specimens with dimensions of $180 \times 180 \times 600$ mm were subjected to combined bending and torsional loading. The test layout is described in detail in [11]. Fig. 4 shows the FE-mesh of the concrete specimen, the support rollers and the load application roller. The concrete specimen and the steel components are discretized by altogether 69372 3D isoparametric 20-node elements with reduced numerical integration.

A notch of isosceles triangular shape of 60 mm length in both vertical and horizontal direction with a notch width of 5 mm was provided at midspan of the specimen at the tensile faces for triggering crack initiation. At an offset of 30 mm from the front face of the specimen a concentrated vertical load was applied to the load application roller, which resulted in combined bending and torsional loading. In the numerical simulation after application of the dead load the concentrated load is applied by prescribing a vertical displacement at a single node of the load application roller.

The material parameters are summarized in Table 2. The uniaxial tensile strength and the specific mode I fracture energy of concrete are estimated according to [10].

The scatter of the experimental results regarding the load-crack mouth opening curve and the respective mean value as well as the numerical results for the PCT-3D test are

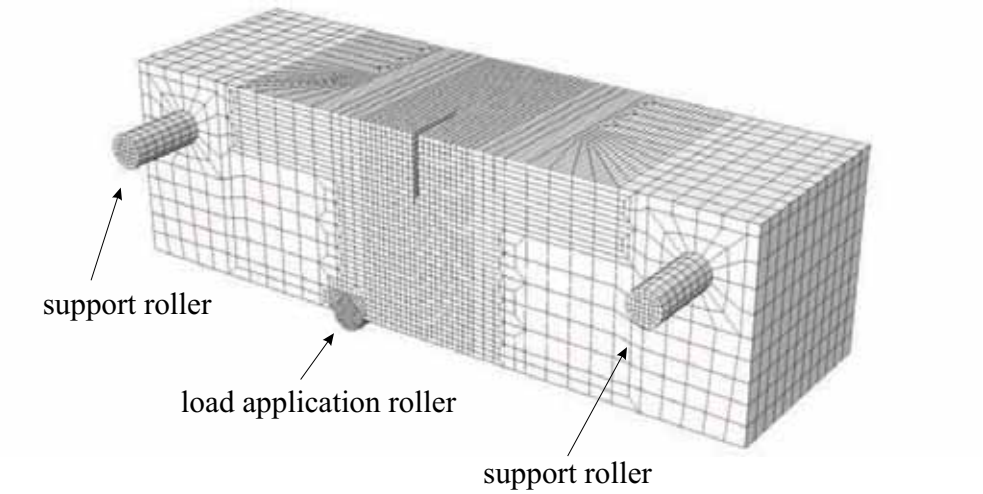

Figure 4: Finite element mesh of the PCT-3D test

Table 2: Material parameters for the numerical simulation of the PCT-3D test

concrete				steel		
param.	mean value		stand. dev.	param.	mean value	
ρ_c	2449	kg/m^3		ρ_s	7850	kg/m^3
E_c	37292	N/mm^2	$\pm$ 2055	E_s	210000	N/mm^2
ν_c	0.19		$\pm$ 0.014	ν_s	0.30	
f_{cu}	40.1	N/mm^2	$\pm$ 0.83			

shown in Fig. 5. In the numerical simulation the onset of cracking is predicted at the center of the base of the triangular notch. With increasing vertical displacement of the point of load application, the crack starts propagating along the base of the triangular notch and subsequently along the top face towards the rear face. At peak load the predicted crack extends from the notch to the rear side of the specimen. In contrast to the front face, at the top face the crack propagates in one row of elements (see Fig. 6). However, in the experiments a slightly curved crack was observed at the top face. Hence, the present model shows some mesh induced bias as a consequence of the employed smeared crack approach. Nevertheless, the overall structural behavior is predicted very well by the present model.

5 CONCLUSIONS

The comparison of the response of two constitutive models for concrete, consisting of a modified version of the Extended Leon model by Pivonka and the damage-plasticity model by Grassl and Jirásek, conducted for several sets of experimental material data, clearly revealed the superiority of the damage-plasticity model. Both models were implemented

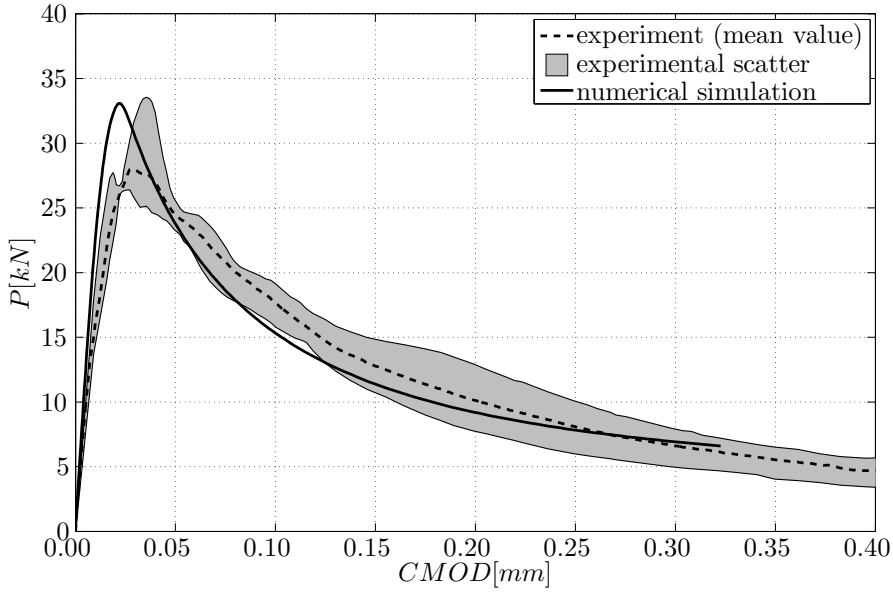

Figure 5: Measured and computed load-crack mouth opening displacement curves for the PCT-3D test

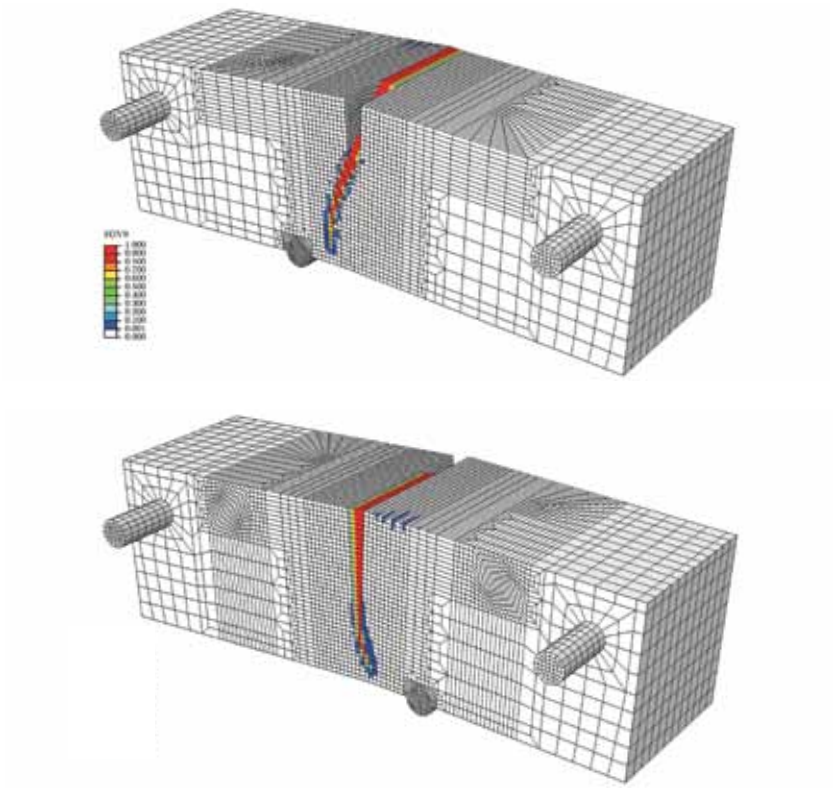

Figure 6: Predicted crack pattern at failure of the PCT-3D test ($SDV9 \equiv \omega$, deformations 50-fold magnified)

into the commercial finite element program ABAQUS, employing the return mapping algorithm, enhanced by substepping and error control, for the stress update. Several benchmark tests conducted on concrete specimens with loadings producing pronounced 3D stress states were analyzed to thoroughly check both the model response and the robustness of the stress update algorithm. The benchmark tests confirmed the capabilities of the enhanced version of the damage-plasticity model for solving large-scale problems in Civil Engineering. An example for the latter is the numerical simulation of an ultimate load test on a 3D model of a concrete arch dam on a scale of 1:200. It allowed a comparison of the predicted response with test data. The finite element mesh, shown in Fig. 7, comprises both the arch dam and the adjacent rock foundation. It consists of about 267 000 3D linear finite elements with altogether 914 000 degrees of freedom. The test setup, the numerical model and the comparison of the predicted response with the test data are described in detail in [8].

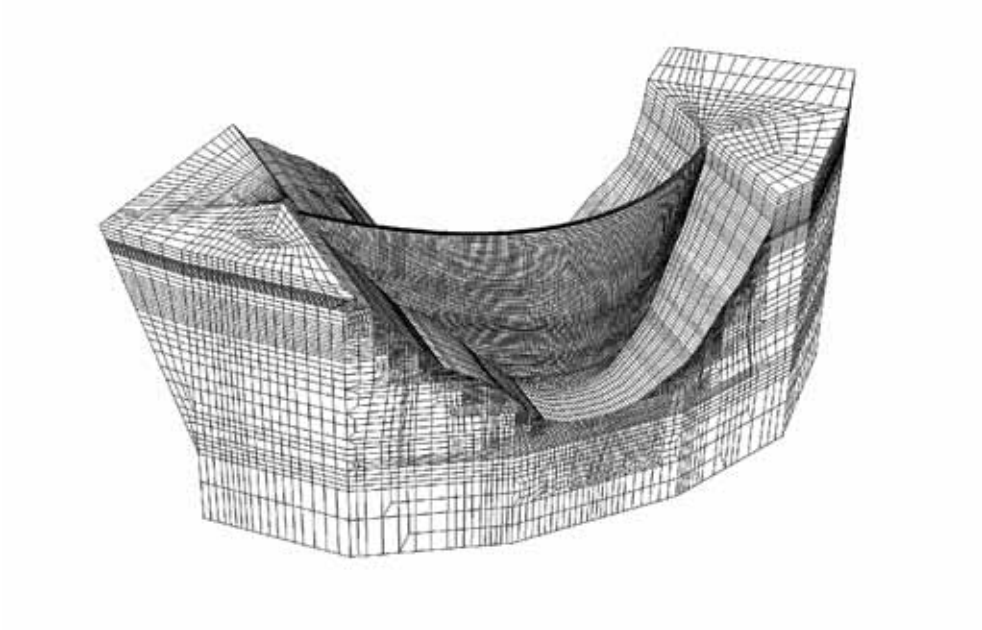

Figure 7: Finite element mesh of the arch dam model

REFERENCES

[1] Etse, G., and Willam, K., Fracture energy formulation for inelastic behavior of plain concrete, *J. Eng. Mech.* (1994) **120**: 1983-2011.

[2] Pivonka, P., Constitutive modelling of triaxially loaded concrete considering large compressive stresses: application to pull-out tests of anchor bolts, *Ph.D.-thesis*,

Vienna University of Technology, Austria, 2001.

[3] Schütt, J., Ein inelastisches 3D-Versagensmodell für Beton und seine Finite-Element-Implementierung, *Ph.D.-thesis*, University of Karlsruhe, Germany, 2005.

[4] Huber, F., Nichtlineare dreidimensionale Modellierung von Beton- und Stahlbetontragwerken, *Ph.D-thesis*, University of Stuttgart, Germany, 2006.

[5] Grassl, P., and Jirásek, M., Damage-plastic model for concrete failure, *Int. J. Solids & Struct.* (2006) **43**: 7166-7196.

[6] ABAQUS User's Manual. Dessault Systemes Simulia Corp., Providence, RI, USA, 2009.

[7] Pérez-Foguet, A., Rodriguez-Ferran, A., and Huerta, A., Consistent tangent matrices for substepping schemes, *Comp. Meth. Appl. Mech. Eng.* (2001) **190**: 4627-4647.

[8] Valentini, B., A three-dimensional constitutive model for concrete and its application to large scale finite element analyses, *Ph.D. thesis*, University of Innsbruck, Austria, 2011.

[9] Imran, I., and Pantazopoulou, S.J., Experimental Study of Plain Concrete under Triaxial Stress, *ACI Material Journal* (1996) **93**: 589-601.

[10] CEB-FIP model code 1990. Bulletin information 203 du Committee Euro-International du Beton, 1991.

[11] Feist, C., and Hofstetter, G., Validation of 3D crack propagation in plain concrete. Part I: Experimental investigation - the PCT3D test, *Computers & Concrete* (2007) **4**: 49-66.